water

MDPI

Article

Hydrothermal Fluids and Cold Meteoric Waters along Tectonic-Controlled Open Spaces in Upper Cretaceous Carbonate Rocks, NE-Iraq: Scanning Data from In Situ U-Pb Geochronology and Microthermometry

Namam Salih [1,2,*], Howri Mansurbeg [3,4], Philippe Muchez [5], Axel Gerdes [6,7] and Alain Préat [8]

1 Petroleum Engineering Department, Engineering Faculty, Soran University, Soran-Erbil 44008, The Kurdistan Region, Iraq
2 Scientific Research Centre (SRC), Soran University, Soran-Erbil 44008, The Kurdistan Region, Iraq
3 General Directorate of Scientific Research Center, Salahaddin University-Erbil, Erbil 44001, The Kurdistan Region, Iraq; howri.mansurbeg@gmail.com
4 School of the Environment, University of Windsor, Windsor, ON N9B 3P4, Canada
5 KU Leuven, Department of Earth and Environmental Sciences, Celestijnenlaan 200E, B-3001 Leuven, Belgium; philippe.muchez@kuleuven.be
6 Institute for Geosciences, Goethe-University Frankfurt am Main, Altenhöferallee 1, 60438 Frankfurt, Germany; gerdes@em.uni-frankfurt.de
7 Frankfurt Isotope and Element Research Center (FIERCE), Goethe-University Frankfurt, 60323 Frankfurt, Germany
8 Research Group.—Biogeochemistry & Modelling of the Earth System, Université Libre de Bruxelles, 1050 Brussels, Belgium; alain.preat@ulb.be
* Correspondence: namam.salih@soran.edu.iq; Tel.: +964-750-460-5345

Abstract: The Upper Cretaceous carbonates along the Zagros thrust-fold belt "Harir-Safin anticlines" experienced extensive hot brine fluids that produced several phases of hydrothermal cements, including saddle dolomites. Detailed fluid inclusion microthermometry data show that saddle dolomites precipitated from hydrothermal (83–160 °C) and saline fluids (up to 25 eq. wt.% NaCl; i.e., seven times higher than the seawater salinity). The fluids interacted with brine/rocks during their circulation before invading the Upper Cretaceous carbonates. Two entrapment episodes (early and late) of FIs from the hydrothermal "HT" cements are recognized. The early episode is linked to fault-related fractures and was contemporaneous with the precipitation of the HT cements. The fluid inclusions leaked and were refilled during a later diagenetic phase. The late episode is consistent with low saline fluids (0.18 and 2.57 eq. wt.% NaCl) which had a meteoric origin. Utilizing the laser ablation U-Pb age dating method, two numerical absolute ages of ~70 Ma and 3.8 Ma are identified from calcrete levels in the Upper Cretaceous carbonates. These two ages obtained in the same level of calcrete indicate that this unit was twice exposed to subaerial conditions. The earlier exposure was associated with alveolar and other diagenetic features, such as dissolution, micritization, cementation, while the second calcrete level is associated with laminae, pisolitic, and microstromatolite features which formed during the regional uplifting of the area in Pliocene times. In conclusion, the hydrothermal-saddle dolomites were precipitated from high temperature saline fluids, while calcrete levels entrapped large monophase with very low salinity fluid inclusions, indicative for a low temperature precipitation from water with a meteoric origin.

Keywords: hydrothermal fluids; cold meteoric waters; Upper Cretaceous carbonate rocks; U-Pb geochronology; fluid inclusion microthermometry

Citation: Salih, N.; Mansurbeg, H.; Muchez, P.; Gerdes, A.; Préat, A. Hydrothermal Fluids and Cold Meteoric Waters along Tectonic-Controlled Open Spaces in Upper Cretaceous Carbonate Rocks, NE-Iraq: Scanning Data from In Situ U-Pb Geochronology and Microthermometry. *Water* **2021**, *13*, 3559. https://doi.org/10.3390/w13243559

Academic Editor: Thomas Meixner

Received: 18 October 2021
Accepted: 6 December 2021
Published: 13 December 2021

1. Introduction

Hydrothermal fluids and meteoric waters are characterized by a significant heterogeneity in geochemical composition. The heterogeneities in composition bring a considerable

challenge for utilizing more sophisticated tools to decipher the origin of the fluids involved during diagenesis, and the burial and temperature history of hydrocarbon reservoirs. To gain better insights into the origin and evolution of these diagenetic fluids, techniques such as conventional petrography, cathodoluminescence, and stable and radiogenic isotopes have been applied [1–6]. The researchers used these methods to understand the complex diagenetic settings in hydrothermal dolomitization. [7] followed a similar approach to identify the conditions which lead to the calcretization of an Upper Cretaceous series in relation with the timing of a dolomitization sequence which was affected by various hot and cold fluids that caused numerous heterogeneities (sensu [8]). Interconnected factors caused a complex heterogeneity in hydrothermal fluids "HT" and cold meteoric waters, including: the source of the fluid's influx/reflux into the host rocks; the amount of hot or cold waters; tectonics; depositional settings; and the interaction of these fluids, especially HT fluids with other stratigraphic sequences prior to the circulation through the final host rocks—all of these processes led to generate a complex pattern [9,10].

This study deals with the origin and composition of the fluids flowing along deep-seated faults through the Upper Cretaceous host rocks of the Bekhme formation (Figure 1). In HT fluids, usually the researchers follow the classical studies, starting from a wide descriptive scenario with analytical techniques to draw the conceptual models for understanding the relative timing of these fluids/waters or their origin [11]. However, the interpretation of these HT fluids remains controversial and fundamental questions remain unanswered. Previously and some recent studies interpreted HT as one phase based on general stratigraphy and structures of the studied area [8,12], while a recent study estimated the absolute age of these fluids by utilizing a laser ablation technique (U-Pb dating [7]). The crucial question, which needs elaboration is the nature and distribution of several HT phases that took place through the circulation of HT fluids with significant variation of salinities. One of the major questions is to determine the number of pulses and the injection age of these HT fluids, in order to unravel the possible driving mechanisms for their upward flow [13].

This study in the Upper Cretaceous Bekhme carbonate formation along Harir-Spelek Basin in the Zagros fold-thrust belt (ZFTB) will add new data to the previous studies in the same area [7,8] to follow the origin of these HT fluids by integrating conventional petrography (including cathodoluminescence) with detailed fluid inclusion petrography, microthermometry, laser ablation "LA" U-Pb dating, and stable isotopes, to constraint paleotemperatures and paleosalinities of the dolomitizing fluids. U-Pb dating is particularly useful to determine the pulse chronology and their possible sources.

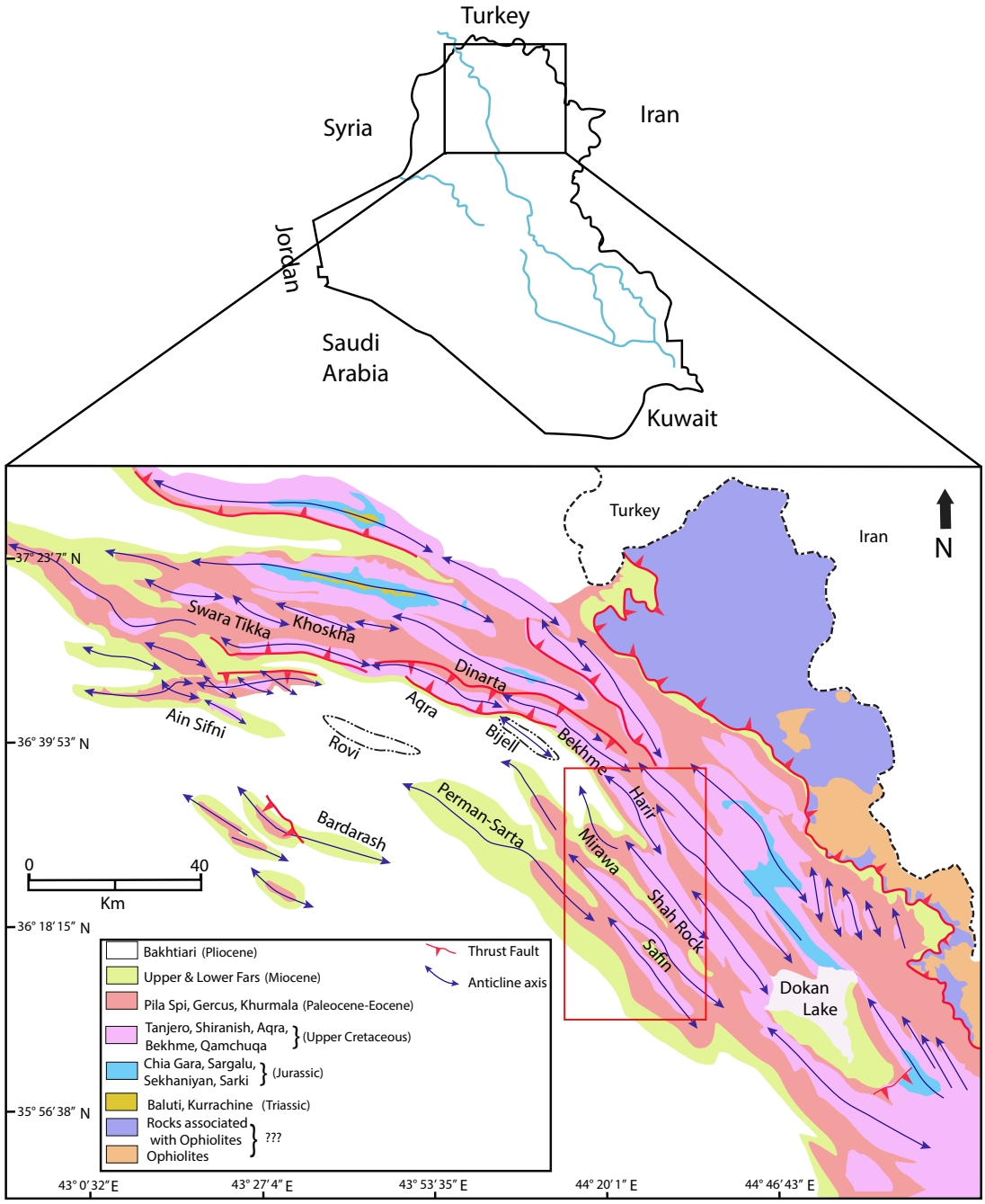

Figure 1. Geological and tectonic map showing the general location of the studied areas "Spelek-Sulauk", see red rectangle (after [7]).

2. Geological Setting

The study area is located within the Zagros fold-thrust belt (ZFTB), Kurdistan Region, northeast Iraq. The area is considered as an important anticlinal structure in the high folded zone, called Harir and Safin anticlines (Figure 1). The study area consists mostly of Upper Cretaceous carbonates at the core of Harir and Safin anticlines, with shallow-water environmental settings [14]. One of the most obvious formations within Cretaceous rocks is the Bekhme formation, which was deposited in a marine shelf environment with rudists, and benthic and planktonic foraminifera [15]. The Bekhme formation is one of the carbonate oil reservoirs in the subsurface and is well exposed to the surface.

During Permian, the opening of the Neotethys oceans started, and was associated with rifting along the ZFTB. The latter underwent complex tectonic events with extensional

phases along both passive margins in the Late Triassic [16]. These extensional phases were followed by the Jurassic–Miocene arc-continent collision and ophiolite obduction along the Arabian plate [17]. Finally, post-orogenic strike-slip faulting progressed and later on the segmentation of Harir and Safin anticlines occurred. The area can be divided into four blocks with a general NW–SE trend. The blocks were controlled tectonically by basement movement along a detachment surface. The strike-slip/oblique faults with a NE–SW trending direction of the Harir and Safin anticlines could reflect the development of a post-orogenic faulting system after the Arabian and Eurasian plate collision.

During the Upper Cretaceous when Bekhme formation was deposited, the basin went through intense tectonic activities, which resulted from the collision between the Arabian and Eurasian plates. The overall tectonic setting shifted from a passive margin to a foredeep setting [18]. The shift in the tectonic regime had a significant impact on the depositional settings and the nature of the sedimentary rocks deposited [18].

3. Materials and Methods

Fluid inclusion petrography and microthermometry were performed on double polished wafers (100–120 µm thick). The wafers were studied under transmitted and fluorescent light in order to distinguish the type of fluid inclusions. Measurements were performed on a Linkam MDS-600 heating-freezing stage(Linkam Scientific Instruments Ltd., Waterfiels, Epsom, Tadworth, UK) mounted on an Olympus BX51 microscope (Olympus Corporation, Tokyo, Japan). The stage was calibrated by measuring synthetic Syn FlincTM fluid inclusion standards (Fluid Inc, Denver, CO, USA). The occurrence of about 110 primary and secondary fluid inclusions were studied under the microscope. The temperatures were obtained by heating and cooling the inclusions in a chamber mounted on a microscope (Table 1). The fluid inclusions present contained two phases, i.e., a liquid (L) and a vapor phase (V). A minimum temperature of the fluid from which a specific mineral precipitated could be obtained during heating. The temperature at which the liquid and vapor phases homogenize is called the homogenization temperature (Th), and is the minimum temperature of entrapment of the fluid inclusion. Freezing and subsequent heating fluid inclusions allow to determine the temperature of first melting of aqueous solid phase and of the final melting. Based on these melting temperatures, the major composition and the salinity of the ambient fluid can be deduced, respectively. The heating rate during homogenization of the fluid inclusions was 3 °C/min and 1 °C/min at the phase transitions during melting. The study and analyses were performed at KU Leuven (Belgium). The preparation technique and measurement procedure have been described by Muchez [19].

Table 1. Distribution and microthermometric data from fluid inclusions. Sp. = Spelek section. Sua. and Sub. = Sulauk sections. Th = homogenization temperature. Tfm = first melting temperature. Tf = freezing temperature. Tmice = final melting temperature of ice. NE-Iraq-Kurdistan Region.

Location	Sample	Rock Phase	Th (°C)	Tf (°C)	Tfm (°C)	Tmice (°C)	Salinity%
Spelek	Sp.16	Saddle Dolomite (SD2)	96	−82	-	−22.3	24.7
			100	−76	-	−20.5	22.7
			100	−76	-	−21.8	23.5
			102	−58	-	−11.9	15.9
			150	−67	-	−23.5	24.7
			150	−65	-	−22.0	23.7
			113	−66	-	−22.4	24

Table 1. *Cont.*

Location	Sample	Rock Phase	Th (°C)	Tf (°C)	Tfm (°C)	Tmice (°C)	Salinity%
			150	−65	-	−22.0	23.7
			113	−66	-	−22.4	24
			102	−69	-	−22.2	23.9
			110	−74	-	−23.0	24.3
			116	−66	-	−21.1	23.8
			86	−74	-	-	-
			120	−69	-	-	-
			121	-	-	-	-
			125	-	-	-	-
			99	-	-	-	-
			141	-	-	-	-
			96	−71	-	−19.7	22.2
			92	−75	−48.6	−20.2	22.5
			94	−74	−45.7	−20.3	22.6
			140	−69	-	−20.3	22.6
			94	-	-	-	-
			94	-	-	-	-
			103	-	-	-	-
			110	-	-	-	-
	Sp.19	**Saddle Dolomite (SD2)**	>150	-	-	-	-
			94	-	-	-	-
			116	-	-	-	-
			99	-	-	-	-
			99	-	-	-	-
			102	-	-	-	-
			95	−75	-	−19.3	21.7
			86	-	-	-	-
			99	−68	-	-	-
			100	−68	-	-	-
			109	−60	-	−14.0	17.8
			>122		-	-	-
			110		-	-	-
			98		-	-	-
			118	−82	-	−19.8	22.2
Sulauk	**Sub.2**	**Late saddle dolomite (SD3)**	116	−78	-	−18.8	21.5
			118	−82	-	−18.8	21.5
			118	−86	-	−21.5	23.4
			119	−83	-	−21.8	23.5
			99		-	-	-
			94	-	-	-	-

Table 1. *Cont.*

Location	Sample	Rock Phase	Th (°C)	Tf (°C)	Tfm (°C)	Tmice (°C)	Salinity%
			96	-	-	-	-
			122	-	-	-	-
			98	-	-	-	-
			98	-	-	-	-
			99	-	-	-	-
			95	-	-	-	-
			109	-	-	-	-
			99	-	-	-	-
			104	-	-	-	-
			122	-	-	-	-
			96	-	-	-	-
			107	−71	-	−20.2	22.5
			100	−74	-	−20.3	22.6
			106	−72	-	−20.5	22.7
			117	-	-	-	-
			108	−62	-	−11.8	15.8
			108	−62	-	−12.2	16.2
			118	−62	−39.8	−12.2	16.2
			109	−62	-	−11.9	15.9
			96	-	-	-	-
			110	-	-	-	-
			86	−63	-	−15.2	18.8
			97	-	-	-	-
			109	-	-	-	-
			110	−60	-	−17.8	20.8
	Sua.3 and Sua.5	**Saddle dolomite (SD3)**	113	-	-	-	-
			104	−70	-	−20.5	22.7
			102	−73	-	−20.5	22.7
			100	−62	-	-	-
			100	−62	-	-	-
			110	−62	-	−13.7	17.5
			110	−62	-	−13.8	17.6
			110	−62	-	−13.8	17.6
			128	−62	-	−16.8	20.1
			86	−82	−41.1	−21.5	23.4
			91	−79	−41.8	−21.6	23.4
			91	−81	-	−21.9	23.6
			86	−78	−41.4	−16.6	19.9
			88	−81	-	−20.8	22.9
			92	−75	-	−17.9	20.9

Table 1. *Cont.*

Location	Sample	Rock Phase	Th (°C)	Tf (°C)	Tfm (°C)	Tmice (°C)	Salinity%
			106	−79	-	−20.8	22.9
			92	−80	-	23.5	24.7
			90	−81	-	−17.6	20.7
			90	−79	-	−22.1	23.8
			102	−77	-	−22.1	23.8
			92	−74	-	−18.6	21.5
			94	−77	-	−16.9	20.2
			108	−79	-	−22.2	23.8
			108	−80	-	−22.2	23.8
			110	-	-	-	-
			103	-	-	-	-
			102	-	-	-	-
			88	-	-	-	-
			93	-	-	-	-
			92	-	-	-	-
			91	-	-	-	-
			90	-	-	-	-
			85	-	-	−21.6	23.4
			92	-	-	−21.9	23.6
			93	−85	-	-	-
Spelek	**Sp. 10**	**Blocky calcite**	Monophase	−39.8		−0.2	0.35
				−37.9		−0.7	1.22
				−39.8		−0.5	0.88
				−37.7		−1.5	2.57
				−39.8		−1.4	2.41
				−39.9		−0.9	1.57
				−39.8		−0.1	0.18
				−37.3		−1.4	2.41
				−39.8		−1.2	2.07
				−41.8		−0.6	1.05
				−39.8		−0.2	0.35
				−40.8		−0.2	0.35

In situ uranium-lead analyses were performed in polished thin sections of dolomite and calcite cements from different samples by laser ablation-inductively coupled plasma-mass spectrometry (LA-ICP-MS) at the Goethe University Frankfurt (Germany). The applied method used an Element2 (Thermo-Scientific, Waltham, MA, USA) sector field ICP-MS coupled to a Resolution ArF excimer laser (Compex Pro 102). The ablated spot size used was 213 µm and depth of the crater was ~20 µm. Samples were screened by LA-ICP-MS for suitable Pb and U concentration and variability. Subsequently, the selected spots were analyzed in fully automated mode overnight. The spot analyses consisted of 20 s background acquisition followed by 20 s of sample ablation. To remove surface contamination prior to analysis, each spot was pre-ablated for 3 s. Soda-lime glass SRM-

NIST 614 was used as a reference glass together with 2 carbonate reference materials, WC-1 and a Zechstein dolomite, to bracket sample analysis (Table 2). The SRM-NIST 614 yielded a depth penetration of about 0.5 μm s^{-1} and an average sensitivity of 280,000 cps/μg g^{-1} for ^{238}U. The detection limits for ^{206}Pb and ^{238}U were ~0.1 and 0.05 ng g^{-1}, respectively. All data were corrected by using MS Excel© spreadsheet program [20,21]. The $^{207}Pb/^{206}Pb$ ratio was corrected for mass bias (0.3%) and the $^{206}Pb/^{238}U$ ratio for inter-element fraction (ca. 5%) using SRM-NIST 614. An additional correction of 4% has been applied on the $^{206}Pb/^{238}U$ to correct for difference in the fractionation due to the carbonate matrix. This resulted in a lower intercept age of 23 WC-1 spot analyses of 254.1 ± 1.5 (MSWD = 1.5; anchored at $^{207}Pb/2^{06}Pb$ of 0.851) and 253.9 ± 3.4 (MSWD = 1.5; n = 17) for the Zechstein dolomite, used as in-house reference material in Frankfurt. Data were plotted in the Tera–Wasserburg diagram and ages were calculated as lower intercepts using Isoplot 3.71 [22]. All uncertainties are reported at the 2-sigma level.

Table 2. Concentration of U-Pb and U-Th-Pb isotopes of reference standards.

Grain	^{206}Pb [a] (cps)	U [b] (ppm)	Pb [b] (ppm)	Th [b] U	^{238}U [c] ^{206}Pb	±2 s (%)	^{207}Pb [c] ^{206}Pb	±2 s (%)
NIST-SRM 614								
NIST614 01	151223	0.81	2.37	0.96	1.241	1.8	0.8714	0.6
NIST614 02	152109	0.82	2.40	0.97	1.230	1.9	0.8711	0.6
Nist614 33	153445	0.81	2.37	0.93	1.240	1.8	0.8662	0.5
Nist614 34	150955	0.81	2.36	0.92	1.244	1.8	0.8730	0.6
Nist614 69	150536	0.81	2.36	0.93	1.246	1.9	0.8700	0.6
Nist614 70	154694	0.82	2.43	0.93	1.226	1.9	0.8705	0.5
Nist614 102	148233	0.80	2.34	0.94	1.237	1.8	0.8696	0.5
Nist614 103	149396	0.81	2.36	0.90	1.238	1.8	0.8714	0.6
Nist614 146	146500	0.80	2.33	0.96	1.240	1.9	0.8728	0.6
Nist614 147	149092	0.81	2.36	0.91	1.241	1.8	0.8693	0.5
Nist614 194	150754	0.82	2.42	0.91	1.234	1.8	0.8734	0.6
Nist614 193	144523	0.81	2.35	0.95	1.247	1.8	0.8766	0.6
Nist614 238	146867	0.81	2.39	0.88	1.232	1.8	0.8709	0.5
Nist614 237	147231	0.82	2.39	0.91	1.230	1.8	0.8651	0.6
NIST614 283	145071	0.82	2.40	0.90	1.237	1.8	0.8670	0.6
Nist614 282	144885	0.82	2.40	0.90	1.236	1.8	0.8719	0.6
NISt614 328	146642	0.84	2.46	0.87	1.240	1.9	0.8700	0.5
Nist614 327	141742	0.83	2.41	0.96	1.244	1.8	0.8751	0.6
NIST614 383	142172	0.84	2.45	0.90	1.243	1.8	0.8685	0.6
Nist614 382	141383	0.83	2.43	0.90	1.235	1.8	0.8713	0.6
NIST614 450	143098	0.86	2.51	0.92	1.235	1.8	0.8730	0.5
WC-1								
Calcite 04	57958	3.60	0.24	<0.001	21.30	2.7	0.1674	4.4
Calcite 03	57442	3.58	0.23	<0.001	21.11	2.1	0.1610	3.2
Calcite 30	53037	3.26	0.22	<0.001	20.98	3.0	0.1761	3.1
Calcite 35	55525	3.55	0.22	<0.001	21.22	2.3	0.1519	3.9
Calcite 36	52116	3.08	0.23	<0.001	20.15	4.0	0.1999	10.8
Calcite 67	60273	3.87	0.24	<0.001	21.96	2.3	0.1595	5.3
Calcite 68	50337	2.99	0.22	<0.001	19.87	3.3	0.2024	9.1
Calcite 102	61659	3.57	0.28	<0.001	19.54	2.7	0.2120	6.8
Calcite 103	55004	3.42	0.23	<0.001	20.82	2.3	0.1874	5.1
Calcite 146	53194	3.33	0.24	<0.001	20.20	4.5	0.1916	6.3
Calcite 147	47066	3.01	0.19	<0.001	21.37	2.5	0.1567	4.9
Calcite 195	53947	3.66	0.23	<0.001	21.43	2.6	0.1489	3.7
Calcite 196	52916	3.60	0.21	<0.001	22.27	2.3	0.1489	3.0
Calcite 239	54507	3.76	0.22	<0.001	22.09	2.3	0.1459	2.8
Calcite 240	56367	3.70	0.24	<0.001	21.39	2.2	0.1842	4.3
Calcite 329	53738	3.63	0.23	<0.001	21.39	2.5	0.1598	6.0

Table 2. *Cont.*

Grain	^{206}Pb [a] (cps)	U [b] (ppm)	Pb [b] (ppm)	Th [b] U	^{238}U [c] ^{206}Pb	±2 s (%)	^{207}Pb [c] ^{206}Pb	±2 s (%)
Calcite 384	50897	3.54	0.23	<0.001	21.21	2.6	0.1747	7.6
Calcite 451	51850	3.55	0.25	<0.001	19.98	4.1	0.1843	10.6
Calcite 285	46761	3.18	0.19	<0.001	22.16	2.2	0.1625	5.2
Calcite 452	52066	3.76	0.24	<0.001	21.40	2.4	0.1612	3.2
Calcitee 507	49116	3.34	0.24	<0.001	20.37	2.5	0.2071	6.5
Calcitee 561	49407	3.65	0.23	<0.001	21.36	2.1	0.1661	4.2
Zechstein dolomite								
ZD 05	383976	2.17	3.12	0.02	2.27	5.5	0.7410	0.6
ZD 37	434820	1.59	3.88	0.02	1.35	4.4	0.7685	0.6
ZD 71	145036	2.03	1.15	0.02	5.22	4.2	0.6482	0.8
ZD 106	98172	1.87	0.82	0.03	6.51	3.2	0.6210	0.9
ZD 150	103377	0.88	0.99	0.05	2.89	2.6	0.7279	0.7
ZD 198	38804	0.90	0.36	0.07	6.60	2.4	0.6067	0.7
ZD 242	15608	0.07	0.16	0.12	1.54	4.2	0.7679	0.9
ZD 287	159760	0.86	1.80	0.08	1.64	8.4	0.7706	0.8
ZD 387	104283	4.59	0.80	0.01	13.05	2.9	0.4131	0.6
ZD 197	90226	2.21	0.72	0.02	8.17	3.9	0.5666	1.2
ZD 241	72961	2.16	0.53	0.02	10.03	3.9	0.4992	1.4
ZD 286	57874	2.37	0.37	0.02	13.71	5.2	0.3945	2.8
ZD 331	66408	2.24	0.49	0.00	10.76	2.4	0.4842	0.9
ZD 386	138406	2.21	1.21	0.02	5.72	3.0	0.6317	0.6
ZD 508	114549	2.26	1.08	0.02	5.96	7.7	0.6264	1.3
ZD 562	99812	2.70	0.90	0.02	8.06	3.5	0.5751	1.3
ZD 385	51470	3.65	0.21	0.00	22.01	2.3	0.1443	3.0

Spot size = 213 µm. ^{238}U/^{206}Pb error is the quadratic additions of the within run precision (2 SE) and excess of variance of 2% (2 SD). ^{207}Pb/^{206}Pb uncertainty propagation as described in Gerdes. Spot size = 213 µm. ^{238}U/^{206}Pb error is the quadratic additions of the within run precision (2 SE) and excess of variance of 2% (2 SD). ^{207}Pb/^{206}Pb uncertainty propagation as described in Gerdes and Zeh (2009). [a]. Within run background-corrected mean ^{206}Pb signal in cps (counts per second). [b]. U and Pb content and Th/U ratio were calculated relative to NIST SRM614 reference. [c]. corrected for background, within-run Pb/U fractionation (in case of ^{206}Pb/^{238}U) and subsequently normal-ized to NIST SRM 614 and carbonate matrix effect of 4% for ^{206}Pb/^{238}U.

4. Results

4.1. Petrography, Cathodoluminescence, SEM, and Stable Isotopes ($\delta^{18}O$ and $\delta^{13}C$)

The Bekhme formation along the Harir-Safin anticlines (NE-Iraq) experienced extensive fracturing, associated with intense hydrothermal fluid migration resulting in zebra-like structures, hydro-brecciation features, and various geodic structures (Figure 2; Salih et al., 2019). The latter authors recognized three phases of saddle dolomites (SD1, SD2, SD3), two phases of blocky calcite cements, and at least three other types of non-saddle dolomites (DI, DII, DIII) inside fractures and geodes.

The DI, DII, and DIII have different sizes and shapes, ranging from anhedral "DI" to euhedral "DIII" crystals (Figure 3A–H), with micritic residues in the core of "DII" and a euhedral shape and transparent color in "DIII" [8]. DIII has a similar dull red luminescence and texture as DI and DII. The micritic residues in "DII" show a spotted red luminescence. The saddle dolomites (SD2 and SD3) display different luminescence patterns ranging from a red luminescence in the cores to a bright red luminescence along the crystal cortices. The blocky calcite crystals, also reported as a hydrothermal product similar to the SD dolomites, have different characteristics, and cathodoluminescence petrography revealed a uniform texture, a dull orange to red luminescence [8].

Calcretized carbonate rocks were a widespread diagenetic feature in the lower and the middle most parts of the Bekhme formation. At least two pedogenic levels were identified based on the presence of typical calcrete features [8]. The vertical variability of pedogenic levels highlights a repeated occurrence of 2–6 m thick calcrete profiles interbedded within a 15–22 m thick succession belonging to the Bekhme formation.

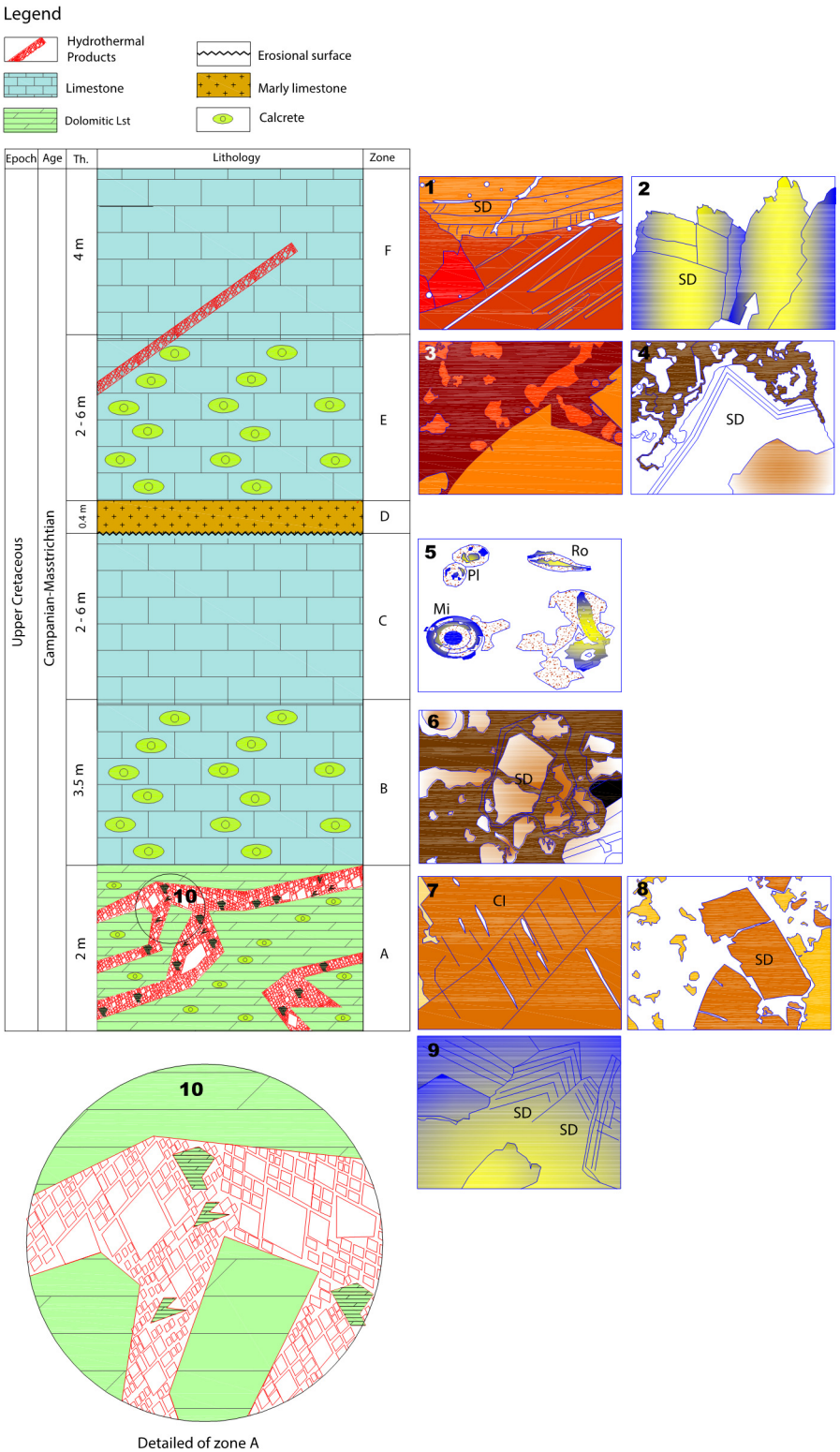

Figure 2. Litho-log of the Bekhme formation from the Spelek-Sulauk area, and next to each zone the digitized microphotographs illustrating the significant alteration of the carbonate rocks. The log shows the emergence (zones B and E) and submergence (zones C and F) of the host carbonate rocks. At least two generations of HT fluids paved their ways along the weakness zones of the host rocks (zones A, E, F). Note the enlarged part (No. 10) of the first generation of HT fluid (zone A), the so-called breccia illustrating the floated, angular grains of the matrix dolomite that is cemented by saddle dolomite. Note another type of brecciation by pedogenic calcrete that caused an in situ fragmentation

of the saddle and matrix dolomites (No. 3, 6, 8). The HT cementation happened prior to the strong in situ brecciation of saddle dolomites (No. 3, 4, 8). Photomicrographs (No. 1, 2, 7, 9) are illustrating unaltered hydrothermal products, while photo No. 4 shows alveolar texture (the brown color on the left part) along the weak joints of the saddle dolomite crystals. The process of alveolar formation is illustrated in photo No. 6; the blue layers define successive layers of dark micrite around fragmented dolomite and show that a non-sequential process of coating starts with an individual tube, followed by a combination of two tubes, until several adjacent tubes are bundled in a micrite coating giving a quasi-concentric structure. CI = blocky calcite, SD = saddle dolomites, Mi = Miliolid, Ro = Rotalid, Pl = Planktonic foraminifera (after [8]).

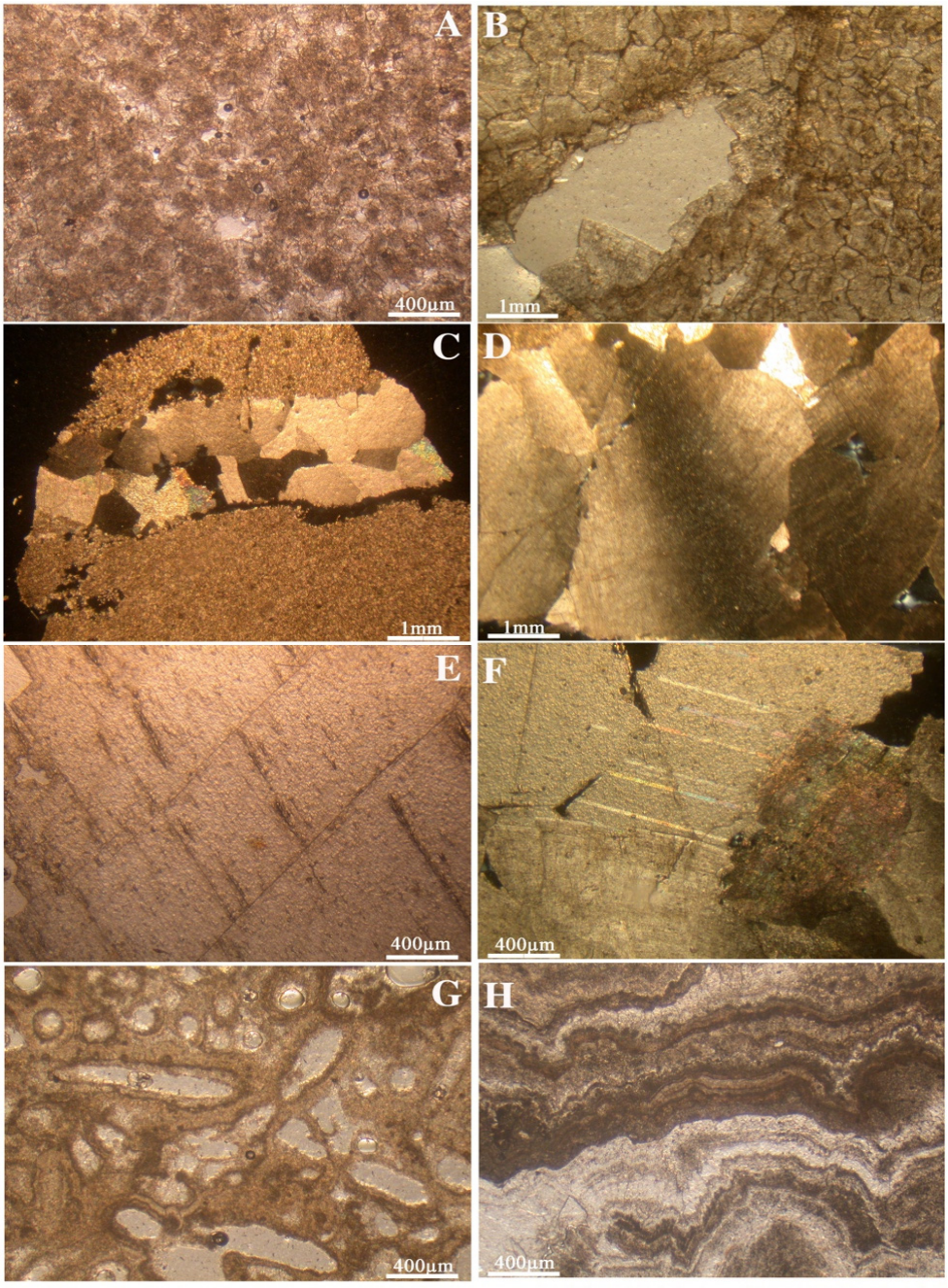

Figure 3. Photomicrographs of carbonate phases. (**A**,**B**) Thin section, polarized light illustrates DI, DII, and DIII dolomites. (**C**,**D**) Thin section under crossed nicols represented the saddle dolomites filling the fracture SD1 (**C**) and void spaces SD2 (**D**). (**E**,**F**) Blocky calcites under PPL (**E**) and XPL (**F**). Calcrete products show two kinds of features: an alveolar texture (**G**) and a pisolitic texture (**H**).

The in situ brecciation due to microbial diagenesis led mostly to alveolar textures, *Microcodium*, and a microbial alteration of the original substrate. A wide spectrum of diagenetic features, such as dissolution, micritization, cementation and re-cementation, dissolution and reprecipitation replacement, grain-to-grain solution, and wall-bridging and open-space fillings have been described [8]. All these features support an in situ pedogenic alteration during subaerial exposure (Figure 3G,H).

All the C-O values used in this study were derived from published data from the same formation and locations [7,8]. All published values from the latter authors have been integrated in this study in order to constrain diagenetic signals based on different recent approaches. The $\delta^{18}O_{VPDB}$ and $\delta^{13}C_{VPDB}$ isotopes gave a narrow range for host limestone and recorded a heavy isotopic composition (varying between −6.7‰ and −4.1‰ for oxygen and 0.3‰ to 1.7‰ for carbon) compared to diagenetic phases (ranging between −17.5‰ and −6.1‰ for oxygen, −6.9‰ and +2.5‰ for carbon). The $\delta^{18}O_{VPDB}$ and $\delta^{13}C_{VPDB}$ values of the calcrete and calcretized samples ranged between −17.8‰ and −6.5‰, and −9.6‰ and 2.5‰, respectively [7,8].

Fragmentation of saddle dolomites floating in the alveolar texture was the most significant feature recognized in the altered saddle dolomites and blocky calcites, and indicates calcretization post-dated saddle dolomite precipitation.

4.2. Petrography of Fluid Inclusions

The study of fluid inclusions (FIs) was carried out on both saddle dolomite and blocky calcite cements (Table 1). Based on the presence, occurrence, and size of the fluid inclusion suitable cements were (i) saddle dolomites SD2 and (ii) SD3, and (iii) blocky calcites CI.

Fluid inclusions in the dolomite and calcite are ubiquitous and included monophase (liquid–L), bi-phase (liquid-vapor, L-V), and sometimes 3-phase (liquid-liquid-vapor L-L-V) inclusions. Two types of FIs were observed in saddle dolomite: primary FIs which were trapped during crystal growth (Figure 4A–C) and secondary FIs which formed after crystal growth (Figures 4A,B and 5A,B). FIs of primary origin occurred in growth zones or in clusters in the crystals (Figure 5C), such as in the core of the dolomite rhombs. Secondary inclusions occurred along trails or in cleavage planes, were frequently larger (up to 40 μm) compared to the primary FIs (up to 20 μm). Due to their small sizes and the darkness of the dolomite crystals, it was very difficult to measure fluid inclusions in the dolomites. The volume of vapor phase varied between 15–25% within the two-phase aqueous inclusions.

Blocky calcite CI was more transparent in comparison with the saddle dolomites. Secondary fluid inclusions were abundant and easily recognized in these blocky calcites. FIs displayed a wider range in size than the dolomite inclusions (measured inclusions range between 15 μm up to >100 μm; Figure 5). The aqueous inclusions (Figure 4A,B) frequently occurred in trails of variable direction, and most of the studied aqueous fluid inclusions were mono-phase. The inclusions displayed a wide range of shapes, from ellipsoidal, simple to irregular. In our study, we measured both primary in saddle dolomites and large secondary monophase FIs in blocky calcite. Since the mono-phase fluid inclusions have no homogenization temperature that can be measured, the final melting temperature of ice and thus the salinity of the inclusions can be measured after artificial stretching of the inclusions.

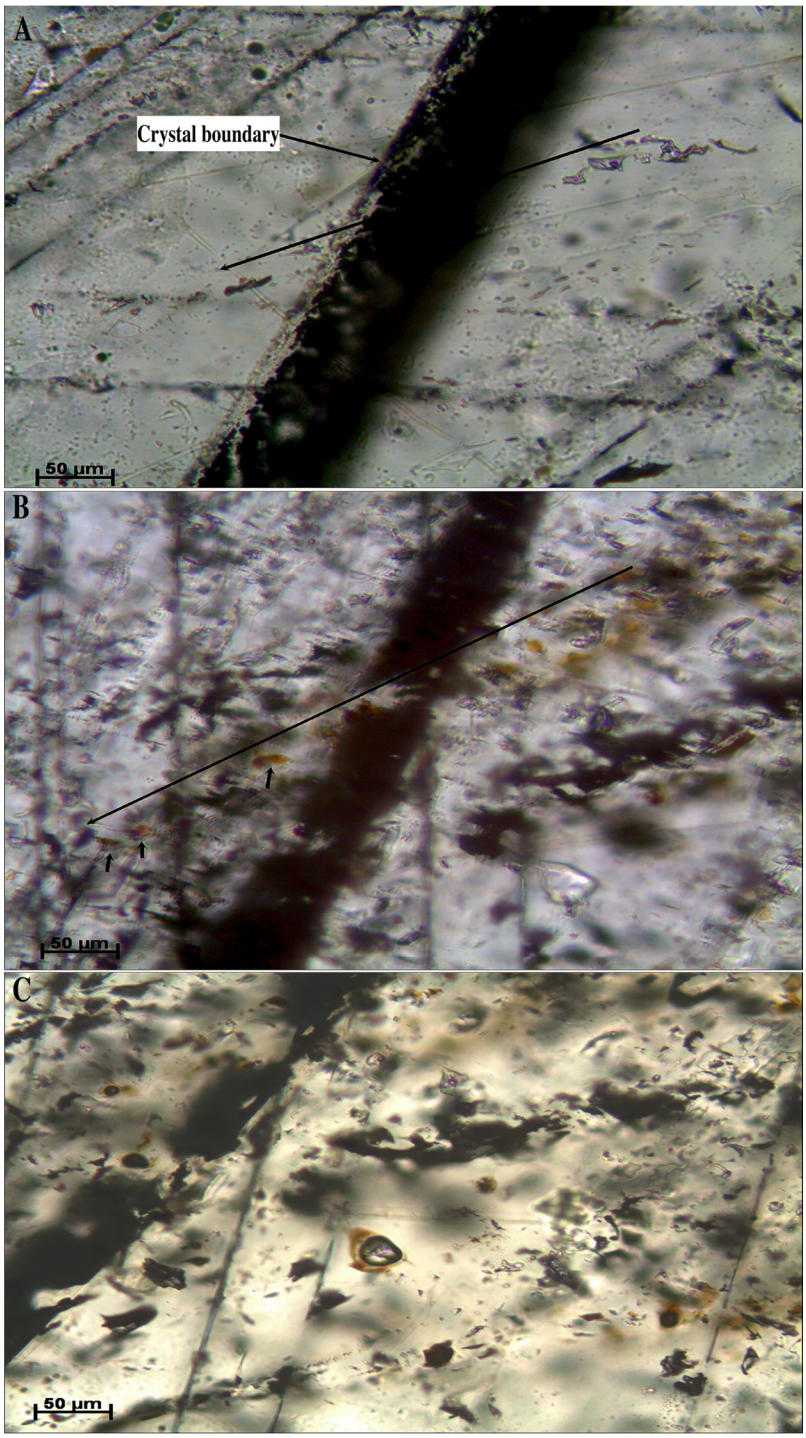

Figure 4. Photomicrographs showing aqueous FIs within the blocky calcite: (**A**) Secondary aqueous FIs crossing the crystal boundary of the blocky calcites (arrow) indicate these inclusions were entrapped after the calcite crystal growth, in addition to small-sized primary FIs. Sua.7. Sulauk section. (**B**) Secondary fluid inclusions crossing the boundary of a calcite crystal, close up the upper right part of the photo that shows the primary FIS. Sulauk section. (**C**) Two-phase primary fluid inclusion. Sua.7. Sulauk section.

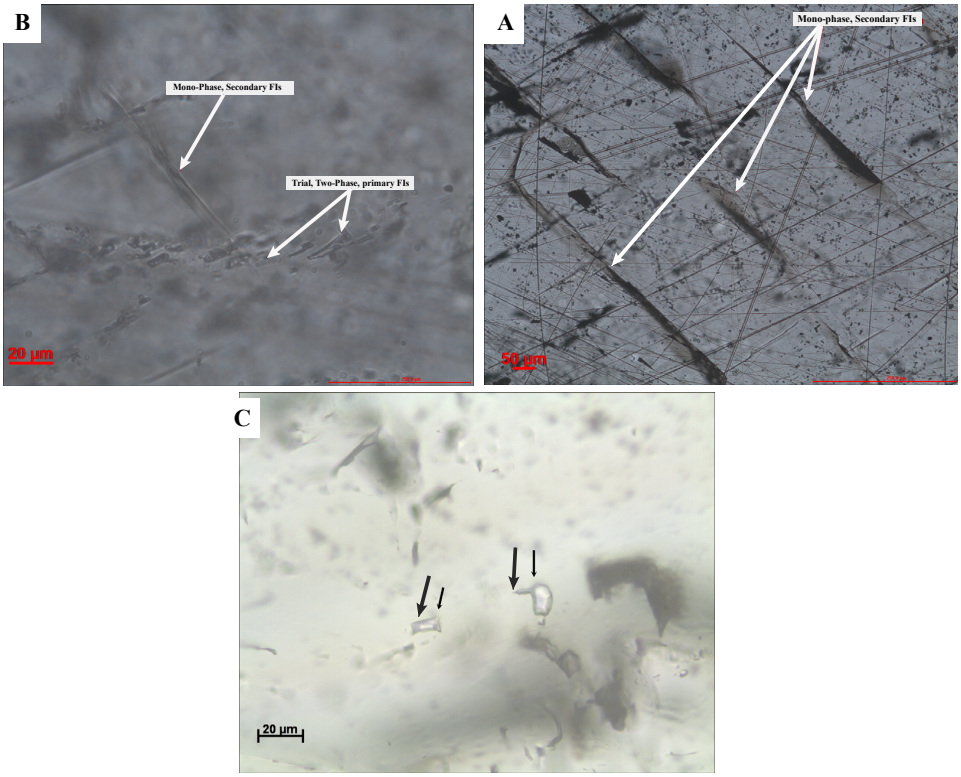

Figure 5. Photomicrographs illustrating one- and two-phase inclusions in the Spelek-Sulauk areas. (**A**,**B**) Secondary, late fluid inclusions in the blocky calcite. (**C**) Primary one-phase and two-phase fluid inclusions (see the black arrows). Sp.10. Spelek section.

4.3. Fluid Inclusion Microthermometry

4.3.1. Saddle Dolomite SD2

Homogenization temperatures (Th) of the saddle dolomite-hosted aqueous fluid inclusions ranged between 86 °C and 118 °C (Table 1; Figure 6A). The first melting temperature Tfm ranged between −48.6 °C to −45.7 °C. These values were lower than those for an H_2O-NaCl binary system, and were only slightly higher than the eutectic temperature of ternary H_2O-NaCl-$CaCl_2$ system [23,24]. Ice melting temperatures (Tm_{ice}) of SD2 range between −23.5 °C and −19.3 °C, corresponding to a salinity between 15.9 and 24.7 equivalent weight percent NaCl (eq. wt.% NaCl) (Figure 6). The salinity values were calculated using the equation of Bodnar [25].

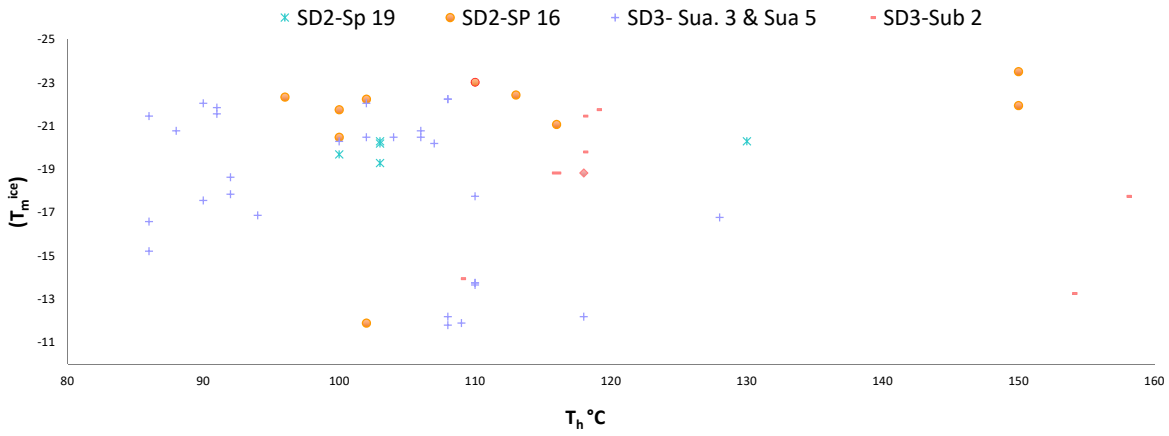

Figure 6. *Cont.*

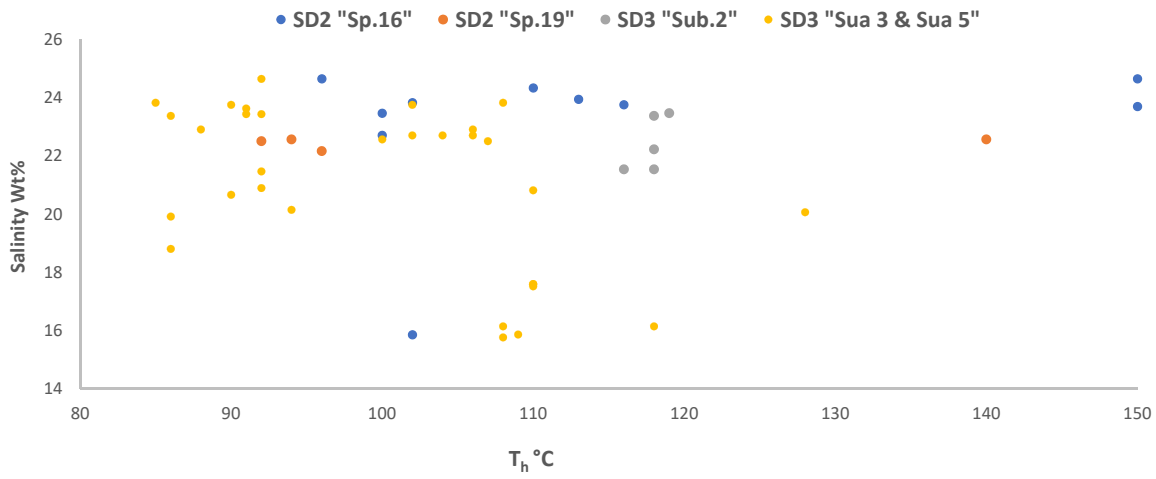

Figure 6. Distribution of homogenization temperatures of the fluid inclusions in the Bekhme formation vs. (**A**) ice melting temperatures (Tmice), and (**B**) corresponding salinities. Sp = Spelek, Sua. and Sub. = Sulauk sections, SD = saddle dolomites.

4.3.2. Blocky Calcites (CI and CII)

CI and CII contained secondary aqueous fluid inclusions. Homogenization temperatures of the FIs in CI were measured on >100 FIs, and showed that generally there are two different types of fluid inclusions, early and late.

Secondary monophase aqueous fluid inclusions were also abundant in blocky calcites. In order to measure their salinities, multiple periods of cooling (up to −100 °C) and heating (up to 200 °C) were carried out to artificially stretch the inclusions and generate a vapor bubble (cf. [26,27]. The monophase secondary FIs yielded a final melting temperature of ice between −0.7 °C to −1.5 °C, corresponding to salinities between 0.2 to 2.6 eq. wt.% NaCl (Table 1). The first melting temperature observed in the fluid inclusions was close to the final melting temperature, which is characteristic for such low salinity inclusions [23].

4.4. U-Pb Dating of the Calcrete

Two samples of calcrete (Sp.3 and Sp.11) were prepared for a LA U-Pb direct dating (Figures 7 and 8; Table 3). Petrographically, sample Sp.3 represents a combination of pure calcrete and chert nodules. Sample Sp.11 displayed an alteration of saddle dolomite inside a geode during the calcretization process. The Pb^{207}/Pb^{206} intercepts at age 3.8 Ma (with σ uncertainties 1.1) and the scatter spot point analyses were outside the isochron with MSWD of 1.9. The pedogenic calcrete and chert nodules from the Spelek sample (Sp.3) yielded a mixing U-Pb age of ~70 Ma for the pedogenic calcrete and ~140 Ma for the chert nodules. Absolute numerical dating results of the same formation of the carbonate cements has been integrated into the recent results that previously reported by Salih [7].

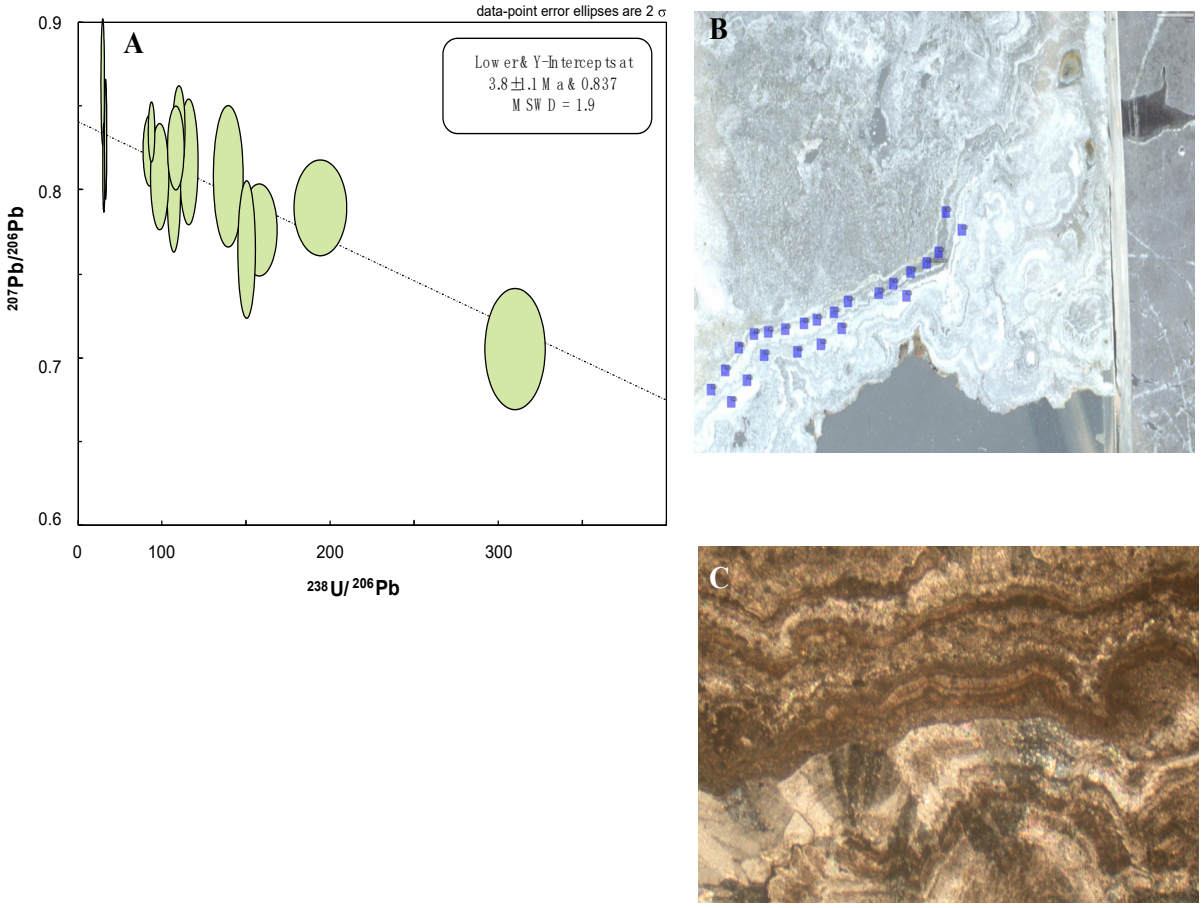

Figure 7. (**A**) The Tera–Wasserburg curve for the analyzed spot points in (**B**). (**B**) Photomicrograph of the ablated spot points inside the geode where saddle dolomite is altered by calcretization process into laminar crust and pisolitic texture. (**C**) The same sample showing the optical characteristics of calcrete features. Sample Sp.11. Spelek section. (n = 24). Harir anticline.

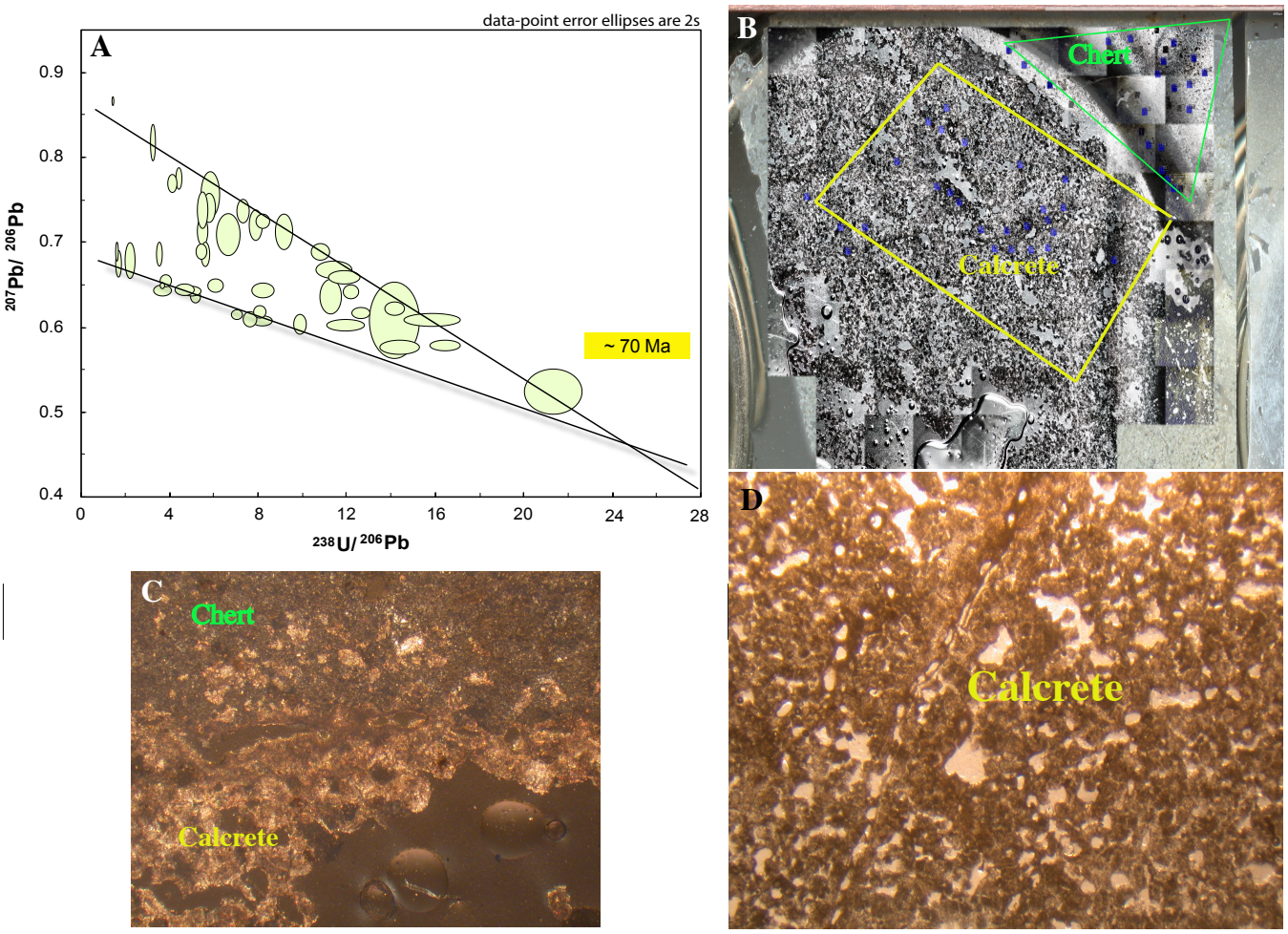

Figure 8. (**A**) The Tera–Wasserburg curve for the analyzed spot points in (**B**), a mixing of two age components in both chert and calcrete is suggested, scatter in the data do not allow to well constrain the age of the two events. (**B**) Photomicrograph showing two subsamples (calcrete and chert), one is an alveolar texture formed as a result of pedogenic calcrete product on the lower part and the center part of the photo (see (**D**)), another subsample located on the upper right part, which represents the location of the chert nodules spot points analysis (see (**C**)). n = 45.

Table 3. Concentration of U-Pb and U-Th-Pb isotopes of host limestone, early dolomite matrix, saddle dolomites, blocky calcites, calcrete, and chert nodules sample by small-scale isochron (SSI) using LAICP-MS approach. Spelek-Sulauk areas. NE-Iraq-Kurdistan region. (n = 190).

Grain	^{206}Pb [a]	U [b]	Pb [b]	Th [b]	^{238}U [d]	±2 s	^{207}Pb [d]	±2 s
	(cps)	(ppm)	(ppm)	U	^{206}Pb	(%)	^{206}Pb	(%)
A172	2196	0.053	0.016	0.006	11.22	3.8	0.6343	2.7
A173	3861	0.056	0.032	0.004	5.425	3.8	0.712	2
A174	4840	0.081	0.038	0.002	6.575	6.6	0.7082	2.9
A175	24795	0.144	0.205	0.008	2.13	8.0	0.6771	2.5
A176	9157	0.086	0.074	0.002	3.473	3.0	0.6851	1.7
A177	7469	0.031	0.060	0.003	1.589	6.9	0.6732	2
A178	6009	0.119	0.052	0.003	7.261	3.0	0.7361	1.6
A179	18528	0.076	0.152	0.003	1.532	3.5	0.6877	1.3
A180	8362	0.125	0.068	0.004	5.538	2.9	0.6846	1.7
A181	4123	0.063	0.035	0.004	5.746	5.8	0.7558	2.9
A182	59898	0.116	0.120	0.005	3.603	9.1	0.6416	0.81
A183	1729	0.102	0.012	0.004	21.29	5.1	0.5217	4.2
A184	5994	0.126	0.051	0.002	7.834	3.0	0.7192	2.1

Table 3. *Cont.*

Grain	^{206}Pb [a]	U [b]	Pb [b]	Th [b]	^{238}U [d]	±2 s	^{207}Pb [d]	±2 s
	(cps)	(ppm)	(ppm)	U	^{206}Pb	(%)	^{206}Pb	(%)
A183	1729	0.102	0.012	0.004	21.29	5.1	0.5217	4.2
A184	5994	0.126	0.051	0.002	7.834	3.0	0.7192	2.1
A185	6869	0.082	0.062	0.003	4.342	2.5	0.7749	1.4
A186	3399	0.084	0.029	0.006	9.108	3.6	0.7117	2.5
A187	3879	0.063	0.036	0.005	5.704	4.0	0.7397	1.9
A188	3489	0.040	0.027	0.009	5.394	3.8	0.7375	2.4
A189	37434	1.660	0.283	0.005	16.41	3.5	0.5762	0.94
A190	48897	1.183	0.408	0.005	8.138	4.5	0.6056	0.83
A191	38268	1.672	0.312	0.004	14.32	5.0	0.5741	1.2
A192	39296	1.507	0.325	0.004	12.96	2.7	0.6087	0.82
A193	144628	0.569	1.540	0.068	1.337	2.0	0.8671	0.48
A199	108990	1.226	0.956	0.011	3.767	5.5	0.6533	0.88
A200	21083	0.255	0.208	0.013	4.048	4.0	0.769	1.1
A201	44634	0.670	0.381	0.014	5.072	3.7	0.6346	1
A202	41916	0.659	0.376	0.008	5.342	3.8	0.6876	1.1
A203	35337	0.810	0.298	0.013	7.576	3.3	0.6075	1.2
A204	46046	0.826	0.404	0.008	5.988	4.8	0.6476	0.99
A205	34360	1.100	0.312	0.005	10.75	3.3	0.6875	1.1
A206	64312	0.934	0.547	0.005	4.934	7.0	0.6407	0.73
A207	58540	1.407	0.498	0.016	8.028	2.8	0.6161	1
A208	35535	1.485	0.299	0.004	14.12	2.6	0.6202	1.1
A209	43572	1.063	0.376	0.005	8.147	5.0	0.6417	1.1
A210	70359	1.446	0.598	0.007	6.963	3.0	0.6131	0.77
A211	48935	1.820	0.407	0.004	12.59	2.6	0.6147	0.86
A212	40903	1.514	0.349	0.004	11.88	6.0	0.6005	0.94
A213	42144	2.265	0.526	0.014	9.835	2.6	0.6014	1.6
A214	70012	0.943	0.594	0.010	4.613	7.7	0.6425	0.85
A215	39667	1.337	0.446	0.004	8.152	3.1	0.7238	0.96
A216	40872	1.952	0.346	0.005	15.83	6.7	0.6067	1
A217	41833	1.414	0.372	0.004	11.36	6.0	0.6665	1.3
A218	36369	1.297	0.323	0.005	11.84	4.9	0.6574	1
A219	33775	1.219	0.292	0.007	12.15	2.4	0.6402	1.1
A220	257672	2.773	2.255	0.006	3.604	2.5	0.6476	0.47
A221	10013	0.094	0.104	0.491	3.166	2.8	0.8176	2.2

5. Interpretation and Discussion

5.1. Fluid Inclusion Petrography and Composition of Fluid Flow

Petrographical observations indicate that saddle dolomites precipitated episodically during an early and late paragenetic sequence, related to subaerial condition and submersion [8]. Saddle dolomites precipitated in two times or phases: Late Cretaceous and Tertiary, the absolute ages for these two phases have been measured by LA U-Pb isotopes and gave numerical absolute ages of 73.8 Ma, and 14.5 and 8.6 Ma [7].

The fluid inclusion petrography shows that most of the measured FIs in the saddle dolomites were aqueous fluid inclusion FIAs. The primary and secondary FIAs were the most dominant types, therefore the FIAs were entrapped during and after the crystal's growth. Therefore, fluid inclusion petrography in saddle dolomites reveals two episodes of entrapments, and thus more than one phase of HT fluid was channeled through the Upper Cretaceous Bekhme formation. However, these two episodes happened at two different times, but still the large-sized secondary (mono-phase) fluid inclusions were trapped at the final stage of diagenesis, since the latter FIs lack the vapor phase and were characterized by large secondary FIs.

The homogenization temperature values from primary and secondary FIAs largely overlapped. The data from both primary and secondary inclusions show that entrapment temperatures of these FIs occurred in two populations (Figures 6 and 9): a first major

population of Th values ranging between 83 °C and 120 °C, and a second minor population with Th values between 130 °C and 160 °C. Lining of fractures and geodes by a first generation of saddle dolomite followed by a second generation of saddle dolomite are consistent with high temperature fluids. At high temperature, an intensive fluid-rock interaction is expected, and such an intense interaction has been reported previously by Salih [3,8] utilizing O-C isotopes. The strongly negative oxygen isotope values (as low as −18‰) and the wide range of O-C values indicate the involvement of several episodes of HT fluid flow through the Bekhme carbonate sequence (Figures 10 and 11). This interaction caused the precipitation of different types of saddle dolomites (SD1, SD2, and SD3) (Figure 3). However, the Th values in saddle dolomites SD2 and SD3 are overlapping (Figure 9). The lowest homogenization temperature (86 °C), however, concerned the earliest precipitated saddle dolomite, while the highest temperature of entrapment was present in a late saddle dolomite (160 °C; Figure 9).

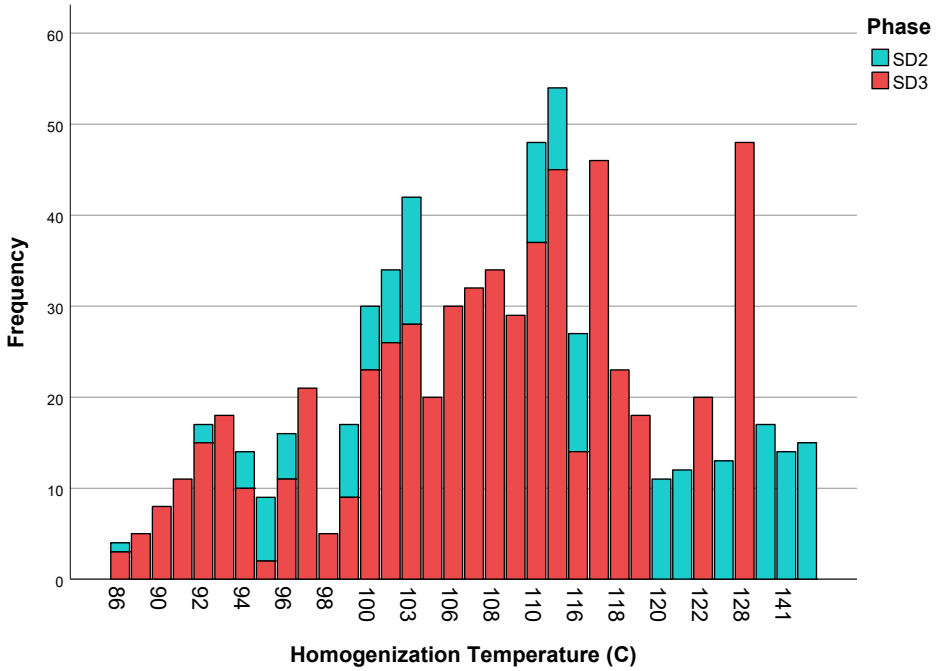

Figure 9. Th data from primary and secondary fluid inclusions in the saddle dolomites and blocky calcite cements vs. frequency from the Spelek-Sulauk area. Each color represents data from different diagenetic phases (n = 102).

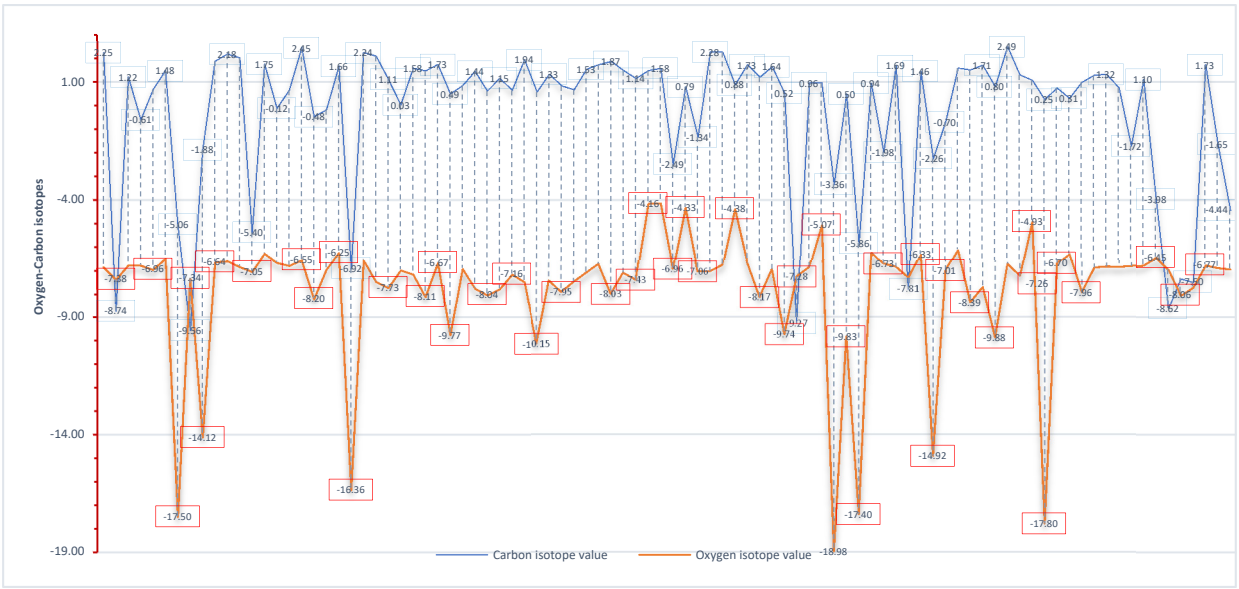

Figure 10. Oxygen and carbon isotopic compositions of carbonate rocks of the Bekhme formation and diagenetic phases for each generation of dolomites, calcites, and calcrete deposits (modified after Salih [7,8]).

The highest cluster of salinity (to 25 eq. wt.% NaCl) is seven times the salinity of seawater. Therefore, the flux of these fluids suggests that they originated as sedimentary brines migrating from the deeper subsurface into the Bekhme formation along deep-seated faults. The upward migration of hydrothermal fluids in the subsurface is often related to a tectonic regime that actively pumped fluids repeatedly during the reactivation of fault systems [7]. The intensive fracturing and the hydraulic breccias in the study area could confirm the involvement of a tectonic regime causing the recorded increase of the Th values in the FIs analyses of the saddle dolomites. The cement's filling open spaces were previously documented as an extra-light value of $\delta^{18}O$ and $\delta^{13}C$ and reported that the fluids involved in precipitation of these cements were hydrothermal fluids (see Figures 10 and 11). Therefore, the following observation and data are considered as indicative of intensive and episodic reactivation of tectonic movement and significant variation was present in the composition of hydrothermal fluids: (i) precipitation of multiple saddle dolomites; (ii) fluctuation of homogenization temperatures (e.g., wide range of paleotemperatures) in FIs trapped in the saddle dolomites, and (iii) saddle dolomites evidencing a consistent fluid origin; (iv) the intensive and moderate interaction with different lithological units in the sequence (based on stable isotope data) and the wide distribution range of oxygen-carbon isotopes (Figure 11).

Recently, a radiometric study also provided a precise time frame using micro-laser ablation technique by ICP-MS on dolomites and calcites hosted in the Upper Cretaceous carbonates [7]. The authors identified more than one type of hydrothermal fluids that altered the Upper Cretaceous Bekhme carbonates and gave an absolute numerical age within the Maastrichtian and Tertiary time interval. The occurrence of a complex fracture network, hydrothermal breccia, geodes, and other open spaces are generally related to more than one faulting system in the study area [8].

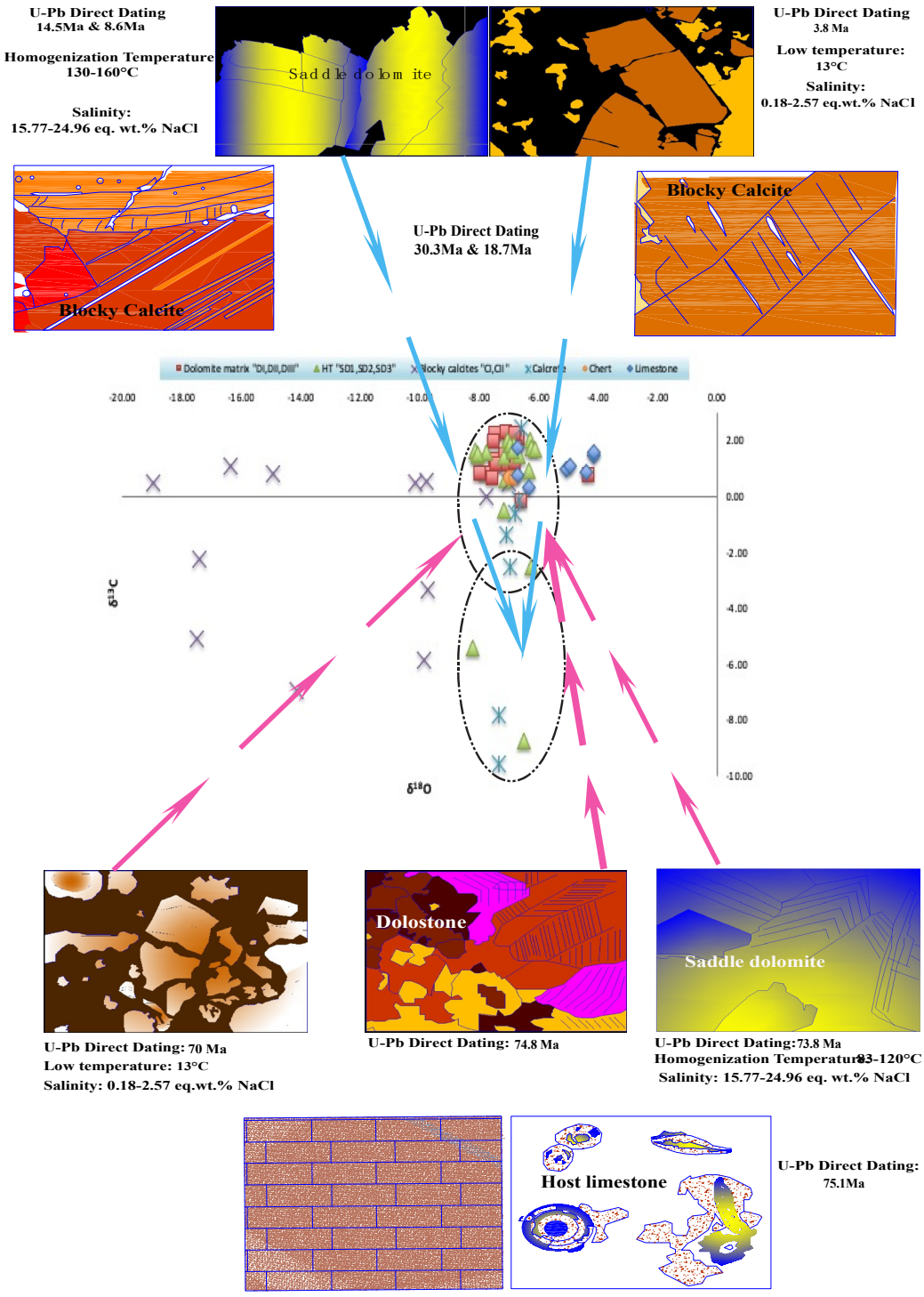

Figure 11. Radiometric model integrated with petrographic and geochemical data to illustrate the absolute age and chemistry of dolomitizing fluids and host rocks during and after the depositional time.

5.2. Thermal Re-Equilibrium, Paleotemperatures in Repeated Hydrothermal Fluids

Fluid inclusion microthermometry, and stable isotopes data provide detailed information on the evolution of temperature and fluid compositions of the HT carbonates, matrix dolomite, and calcrete products. The homogenization temperatures from saddle dolomite samples cover a considerable range of values. More than 95% of all measured primary and secondary fluid inclusions point to homogenization temperatures between 83 °C and

118 °C for SD2/SD3. This range represents true syn-entrapping and post-entrapping temperatures during and after mineral growths, either in or out of thermal re-equilibrium.

Chemical and physical factors affecting thermal re-equilibrium processes can produce stretching, leakage, and refilling of the fluid inclusions [24,28]. However, the inability of fluid inclusions to resist a temperature increase of the host rock increases with the size of the inclusions, causing stretching of the inclusions [29]. The current measurements of small-sized inclusions (15–20 μm) with the same Th values as the larger inclusions (up to 40 μm) suggest that "re-equilibrium" of inclusions did not play a major role in our data set.

Multiple events of hydrothermal fluids over time based on bimodal paleotemperature distributions are documented throughout the Permo-Triassic and Carboniferous sections in the West of Britain and Ireland [30]. Consequently, the wide and high-recorded temperatures (83–160 °C) in our study may reflect either multiple pulses of hydrothermal fluids (cf. [31]) or a fluid evolution in the context of a long-lived hydrothermal system [32]. An evolution of the hydrothermal fluids over long periods of time (long-lived HT fluids, cf. [33]) is linked to a considerable range of salinity composition and associated with relatively uniform temperature degrees.

5.3. Cold Meteoric Waters' Origin Associated with Hydrothermal Products

High saline fluids and low saline meteoric waters were brought either by deep-seated faults or by exposing the carbonate body to the surface, which resulted in precipitation of different carbonates [8]. The exposure of carbonate to the surface may have brought low saline water into the Bekhme formation, with the trapping of low saline fluid inclusions (0.2 and 2.6 eq. wt.% NaCl). These FIs are trapped as a secondary monophase inclusions in calcite cement, and are indicative of a late episode of diagenesis. These inclusions were entrapped along cleavage planes in calcite, and they crosscut even the boundary of crystal grain (Figure 5). Low saline water involved in the precipitation of this kind of calcite displayed a much lower temperature (around 13 °C, [8]) than the ones of hydrothermal saddle dolomites (83–118 °C). Similar large fluid inclusions were trapped below <50 °C in the Lower Carboniferous of the Variscan foreland of southern Belgium, and these FIs postdated the Variscan orogeny. Fresh water from which these calcites precipitated have a telogenetic origin (e.g., [27,34]). Invariable δ18 O values and variable and negative δ13C values of the calcites studied closely match the inverted J-pattern or curve of meteoric calcites, and therefore a meteoric origin and telogenetic origin is proposed for these late calcites (Figures 10 and 11).

5.4. Radiogenic Isotopes Data Scanning

5.4.1. Timing of Diagenetic Events Utilizing U-Pb Dating

Using the absolute laser ablation ICP-MS U-Pb direct dating, the saddle dolomites and blocky calcites originated from hydrothermal fluid and occurred at least in two major phases (Cretaceous 73.8 Ma and Tertiary, not older than 30.8 Ma [7]). These meaningful ages overlap with an estimated age of the studied Upper Cretaceous carbonate (75.1 Ma) (Figure 11). Visual and optical characteristics of carbonates show evidence of microbial alteration on the surface due to the ancient activity of fungal and bacterial colonization [8].

U-Pb dating of calcrete samples "Sp.3 and Sp.11" yielded two ages: ~70 Ma and 3.8 Ma. According to Gradstein [35], these numerical absolute ages are well consistent with the Campanian and Pliocene periods. Calcrete sample Sp.3 with a clear alveolar texture gives a Campanian age of ~70 Ma. The numerical absolute age "~70 Ma" is equivalent to the interval age of the Bekhme depositional carbonates (Campanian-Early Maastrichtian age). The pisolitic and laminar crusts of the calcrete (with a lack of pedogenic products, e.g., alveolar texture) on the altered saddle dolomite yielded a U-Pb age of 3.8 Ma. This age of 3.8 Ma records the last event of the diagenetic history in Upper Cretaceous carbonates.

Based on these two different events, the first one (~70 Ma) is in good agreement with the estimated age of Bekhme formation, while the second one brings new insight, indicating that a young diagenetic phase affected the whole Bekhme formation. This diagenetic event

could have coincided with the migration of a low saline fluid (0.2 and 2.6 eq. wt.% NaCl) recorded in the blocky calcites. The uplifting of the area during a major tectonic event in the Pliocene could have caused widespread infiltration of meteoric water, whose salinity increased due to the interaction with the host rock, and mixing with higher salinity fluids, still present in the pores. The Pliocene recorded the greatest rate of erosion in the high folded zone [36].

Combining petrography, O-C isotopic, and U-Pb data, first by tying the two calcrete types with oxygen-carbon isotope compositions, shows that the O-C isotope values of the older calcrete (70 Ma) overlap with those of the saddle dolomites and the matrix dolomites (73.8 Ma and 74.8 Ma), in contrast to the younger calcrete (3.8 Ma) which has lighter O-C isotope values (Figure 11).

5.4.2. Timing of Non-Diagenetic and Diagenetic Carbonate Rocks

Using the U-Pb age dating method and by integrating field observations, petrography, and fluid inclusion microthermometry from carbonate rocks, Salih [8] drew a time framework for the host limestone of the Bekhme formation and its diagenetic alteration. The meaningful numerical age of unaltered host limestone (non-diagenetic or pristine) is 75.1 Ma, and corresponds to a Late Campanian age, in good concordance with the interval age of the Bekhme formation [7]. The authors added that in a very short time, the early dolomites replaced the host limestones (~73.8 Ma). Another phase of an HT mineral has an absolute age of Tertiary times. An early HT mineral just postdated the precipitation of matrix dolomite (~74.8 Ma; [7]). Therefore, saddle dolomites and blocky calcites recorded at least two major generations of HT fluids.

Another new diagenetic phase consists of the pedogenic calcrete, which shows an enrichment in uranium isotopes. This enrichment suggests that the sediment 'or calcretized rock', is younger than the other carbonate phases. The numerical absolute age of one sample of the calcrete associated with abundant alveolar textures and other microbial activities gives an age of ~70 Ma, which is close to the Bekhme formation time and possibly the first generation of the HT dolomites. In the case of the U-Pb dating of the second calcrete level with the laminar and pisolitic textures, and without alveolar textures, an age of 3.8 Ma was established (Figure 11).

6. Conclusions

Based on optical characteristics, visual petrography of fluid inclusions and microthermometry, stable isotopes, and U-Pb dating, two main entrapment episodes of aqueous FIs were identified from their optical characteristics at room temperatures;

1. An early entrapment episode of fluid inclusions in HT dolomite cements exhibited a range of homogenization temperatures with (i) a first population of Th values between 83 °C and 120 °C and (ii) a second population with Th values between 130 °C and 160 °C. Both populations showed an overlap in their salinity (mainly between 15.8–25 eq. wt.% NaCl). Their salinity and Th values indicated an episodic upward migration of HT fluids related to tectonic activity;
2. The late entrapment episode of fluid inclusions was associated with secondary monophasic FIs, and recorded a diluted fluid (up to 2.6 eq. wt.% NaCl) under low temperature conditions, which coincided with a calcretization of the carbonate rock;
3. The early migration of high temperature fluids possibly occurred during the Late Cretaceous HT, while the second migration of low saline fluids of meteoric origin was associated with and uplifted during Pliocene times. These two periods of fluid migration provide new insight into the geology of the area studied, i.e., contributing to the relationship between fluid flow and the tectonic movements during the Zagros Orogeny;
4. The two episodes are further supported by LA ICP-MS U-Pb dating. The numerical results indicated an absolute age of the pedogenic calcrete, associated with abundant alveolar textures and other microbial activities, which gave a U-Pb age of ~70 Ma

which is close to the period that the Bekhme formation was deposited. This paragenetic sequence ended by the uplift of the Spelek-Sulauk areas during the Pliocene, which caused calcrete formation. In the case of the U-Pb age dating of the laminar and pisolitic textures, an age of 3.8 Ma was established for the end of the diagenetic event when this sequence was exposed to the surface.

Author Contributions: Writing and preparation the original draft, N.S. and A.P.; review and editing, N.S., A.P., P.M. and H.M.; Methodology and software, G.A., P.M., A.P. and N.S. All authors have read and agreed to the published version of the manuscript.

Funding: The study benefited from research funds of the Université Libre de Bruxelles (ULB)-Belgium.

Acknowledgments: This work was supported by Université Libre de Bruxelles-Belgium and it is FIERCE contribution No. 86.

Conflicts of Interest: The authors declare no conflict of interest.

References

1. Hardie, L.A. Secular variation in seawater chemistry: An explanation for the coupled secular variation in the mineralogies of marine limestones and potash evaporites over the past 600 m.y. *Geology* **1996**, *24*, 279–283. [CrossRef]
2. Mansurbeg, H.; Morad, D.; Othman, R.; Morad, S.; Ceriani, A.; Al-Aasm, I.; Kolo, K.; Spirov, P.; Proust, J.N.; Preat, A.; et al. Hydrothermal dolomitization of the Bekhme formation (Upper Cretaceous), Zagros Basin, Kurdistan Region of Iraq: Record of oil migration and degradation. *Sediment. Geol.* **2016**, *341*, 147–162. [CrossRef]
3. Salih, N.; Mansurbeg, H.; Préat, A. Geochemical and Dynamic Model of Repeated Hydrothermal Injections in Two Mesozoic Successions, Provençal Domain, Maritime Alps, SE-France. *Minerals* **2020**, *10*, 775. [CrossRef]
4. Yoshimura, T.; Wakaki, S.; Ishikawa, T.; Gamo, T.; Araoka, D.; Ohkouchi, N.; Kawahata, H. A Systematic Assessment of Stable Sr Isotopic Compositions of Vent Fluids in Arc/Back-Arc Hydrothermal Systems: Effects of Host Rock Type, Phase Separation, and Overlying Sediment. *Front. Earth Sci.* **2020**, *8*, 595711. [CrossRef]
5. Chi, G.; Larryn, W.D.; Huanzhang, L.; Jianqing, L.; Haixia, C. Common Problems and Pitfalls in Fluid Inclusion Study: A Review and Discussion. *Minerals* **2021**, *11*, 7. [CrossRef]
6. Farsang, S.; Louvel, M.; Zhao, C.; Mezouar, M.; Rosa, A.D.; Widmer, R.N.; Feng, X.; Liu, J.; Redfern, S.A. Deep carbon cycle constrained by carbonate solubility. *Nat. Commun.* **2021**, *12*, 1–9. [CrossRef]
7. Salih, N.; Mansurbeg, H.; Kolo, K.; Gerdes, A.; Préat, A. In situ U-Pb dating of hydrothermal diagenesis in tectonically controlled fracturing in the Upper Cretaceous Bekhme Formation, Kurdistan Region-Iraq. *Int. Geol. Rev.* **2019**, *62*, 2261–2279. [CrossRef]
8. Salih, N.; Mansurbeg, H.; Kolo, K.; Préat, A. Hydrothermal Carbonate Mineralization, Calcretization, and Microbial Diagenesis Associated with Multiple Sedimentary Phases in the Upper Cretaceous Bekhme Formation, Kurdistan Region-Iraq. *Geosciences* **2019**, *9*, 459. [CrossRef]
9. Katz, D.A.; Eberli, G.P.; Swart, P.K.; Smith, L.B. Tectonic-hydrothermal brecciation associated with calcite precipitation and permeability destruction in Mississippian carbonate reservoirs, Montana and Wyoming. *AAPG Bull.* **2006**, *90*, 1803–1841. [CrossRef]
10. Jack, S.; Cathy, H.; Hilary, C.; Ardiansyah, K. Burial dolomitization driven by modified seawater and basal aquifer-sourced brines: 562 Insights from the Middle and Upper Devonian of the Western Canadian Sedimentary Basin. *Basin Res.* **2020**, *33*, 648–680. [CrossRef]
11. Zhu, D.; Liu, Q.; Zhang, J.; Ding, Q.; He, Z.; Zhang, X. Types of Fluid Alteration and Developing Mechanism of Deep Marine Carbonate Reservoirs. *Geofluids* **2019**, *2019*, 1–18. [CrossRef]
12. Davies, G.R.; Smith, L.B. Structurally controlled hydrothermal dolomite reservoir facies: An overview. *AAPG Bull.* **2006**, *90*, 1641–1690. [CrossRef]
13. Lonnee, J.; Machel, H.G. Pervasive dolomitization with subsequent hydrothermal alteration in the Clarke Lake gas field, Middle Devonian Slave Point Formation, British Columbia, Canada. *AAPG Bull.* **2006**, *90*, 1739–1761. [CrossRef]
14. Bellen, V.; Dunnington, H.; Wetzel, R.; Morton, D. Lexique stratigraphique international Asie. *Iraq* **1959**, *3C*, 333.
15. English, J.; Lunn, G.A.; Ferreira, L.; Yacu, G. Geologic evolution of the Iraqi Zagros, and its influence on the distribution of hydrocarbons in the Kurdistan region. *AAPG Bull.* **2015**, *99*, 231–272. [CrossRef]
16. Ismail, S.; Kettanah, Y.; Chalabi, S.; Ahmed, A.; Arai, S. Petrogenesis and PGE distribution in the Al-and Cr-rich chromites of the Qalander ophiolite, northeastern Iraq: Implications for the tectonic environment of the Iraqi Zagros Suture Zone. *Lithos* **2014**, *202*, 21–36. [CrossRef]
17. Ballato, P.; Uba, C.; Landgraf, A.; Strecker, M.; Sudo, M.; Stockli, D.; Friedrich, A.; Tabatabaei, S. Arabia-Eurasia continental 501 collision: Insights from late Tertiary foreland basin evolution in the Alborz Mountains, northern Iran. *Geol. Soc. Am. Bull.* **2011**, *123*, 106–131. [CrossRef]

18. Homke, S.; Vergés, J.; Serra-Kiel, J.; Bernaola, G.; Sharp, I.; Garcés, M.; Montero-Verdú, I.; Karpuz, R.; Goodarzi, M.H. Late Cretaceous-Paleocene formation of the proto–Zagros foreland basin, Lurestan Province, SW Iran. *Geol. Soc. Am. Bull.* **2009**, *121*, 963–978. [CrossRef]
19. Muchez, P.; Marshall, J.D.; Touret, J.L.R.; Viaene, W.A. Origin and migration of palaeofluids in the Upper Visean of the Campine Basin, northern Belgium. *Sedimentology* **1994**, *41*, 133–145. [CrossRef]
20. Gerdes, A.; Zeh, A. Combined U–Pb and Hf isotope LA-(MC-)ICP-MS analyses of detrital zircons: Comparison with SHRIMP and new constraints for the provenance and age of an American metasediment in central Germany. *Earth Planet. Sci. Lett.* **2006**, *249*, 47–61. [CrossRef]
21. Gerdes, A.; Zeh, A. Zircon formation versus zircon alteration—New insights from combined U–Pb and Lu–Hf in-situ LA-ICP-MS analyses, and consequences for the interpretation of Archean zircon from the Central Zone of the Limpopo Belt. *Chem. Geol.* **2009**, *261*, 230–243. [CrossRef]
22. Ludwig, L. *Isoplot 3.7: A Geochronological Toolkit for Microsoft Excel*; Special Publication 4; Berkeley Geochronology Center: Berkeley, CA, USA, 2008; pp. 1–77.
23. Roedder, E. Fluid inclusions. *Rev. Mineral.* **1984**, *12*, 646.
24. Goldstein, H. Fluid inclusions in sedimentary and diagenetic systems. *Lithos* **2001**, *55*, 159–193. [CrossRef]
25. Bodnar, R. Revised equation and table for determining the freezing point depression of H2O-Nacl solutions. *Geochim. Cosmochim. Acta* **1993**, *57*, 683–684. [CrossRef]
26. Goldstein, R.H. Petrographic and geochemical evidence for origin of paleospeleothems, New Mexico: Implications for the application of fluid inclusions to studies of diagenesis. *J. Sediment. Petrol.* **1990**, *60*, 282–292.
27. Muchez, P.; Slobodnik, M. Recognition and significance of multiple fluid inclusion generations in telogenetic calcites. *Min.-Alogical Mag.* **1996**, *60*, 813–819.
28. Bodnar, J. Reequilibration of fluid inclusions. In *Fluid Inclusions—Analysis and Interpretation*; Samson, I., Anderson, A., Marshall, D., Eds.; Short Course Series; Mineralogical Association of Canada: Quebec City, QC, Canada, 2003; Volume 32, pp. 213–231.
29. Goldstein, H.; Reynolds, J. Systematics of fluid inclusions in diagenetic minerals. *SEPM Soc. Sediment. Geol.* **1994**, *545*, 31.
30. Middleton, J.; Parnell, J.; Green, F.; Xu, G.; McSherry, M. *Hot Fluid Flow Events in Atlantic Margin Basins: An Example from the Rathlin Basin*; Special Publications 188; Geological Society: London, UK, 2001; pp. 91–105.
31. Hiemstra, J.; Goldstein, H. *Repeated Injection of Hydrothermal Fluids into Downdip Carbonates: A Diagenetic and Stratigraphic Mechanism for Localization of Reservoir Porosity, Indian Basin Field, New Mexico, USA*; Special Publications 406; Geological Society: London, UK, 2015; pp. 141–177.
32. Tobin, C.; Claxton, L. Multidisciplinary thermal maturity studies using vitrinite reflectance and fluid inclusion microthermom-601 etry, A new calibration of old techniques. *Am. Assoc. Pet. Geol. Bull.* **2000**, *84*, 1647–1665.
33. Dewit, J.; Foubert, A.; Desouky, E.A.; Muchez, P.; Hunt, D.; Vanhaecke, F.; Swennen, R. Characteristics, genesis and parame-ters controlling the development of a large stratabound HTD body at Matienzo (Ramales Platform, Basque Cantabrian Basin, northern Spain). *Mar. Pet. Geol.* **2014**, *55*, 6–25. [CrossRef]
34. Alonso-Zarza, M.; Tanner, H. *Carbonates in Continental Setting: Facies, Environments and Processes, Developments in Sedimentology*; Elsevier: Amsterdam, The Netherlands, 2010; pp. 225–267.
35. Gradstein, M.; Ogg, G.; Schmitz, M.; Ogg, G. *The Geologic Time Scale 2012*; Elsevier: Boston, MA, USA, 2012; p. 1176.
36. Lawa, F.A.; Koyi, H.; Ibrahim, A. Tectono-stratigraphic evolution of the NW segment of the Zagros Fold-Thrust Belt, Kurdistan, NE. *J. Pet. Geol.* **2012**, *36*, 75–96. [CrossRef]